

On autocorrelation analysis of jet noise

Blaine M. Harker, Kent L. Gee, Tracianne B. Neilsen, and Alan T. Wall

Department of Physics and Astronomy, Brigham Young University, Provo, Utah 84602
blaineharker@gmail.com, kentgee@byu.edu, tbn@byu.edu, alantwall@gmail.com

Sally A. McInerny

Department of Mechanical Engineering, University of Louisiana Lafayette,
Lafayette, Louisiana 70504
smcinerny@louisiana.edu

Michael M. James

Blue Ridge Research and Consulting, Asheville, North Carolina 28801
michael.james@blueridgeresearch.com

Abstract: Meaningful use of the autocorrelation in jet noise analysis is examined. The effect of peak frequency on the autocorrelation function width is removed through a temporal scaling prior to making comparisons between measurements or drawing conclusions about source characteristics. In addition, a Hilbert transform-based autocorrelation envelope helps to define consistent characteristic time scales. Application of these processes to correlation functions based on large and fine-scale similarity spectra reveal that the large-scale noise radiation from an F-22A deviates from the similarity spectrum model.

© 2013 Acoustical Society of America

PACS numbers: 43.28.Ra, 43.50.Nm [SS]

Date Received: February 5, 2013 **Date Accepted:** April 11, 2013

1. Introduction

The autocorrelation function is effective in relating waveform properties to spectral features. In jet noise analysis, it has been used to investigate noise source and radiated field characteristics, including waveform periodicities and their connections to temporal and spatial length scales of turbulent structures.¹⁻⁴ These length scales can be used to support models of large-scale structure (LSS) and fine-scale structure (FSS) mixing noise. However, before making conclusions regarding source or field properties, current analysis techniques need to be examined. The principal purpose of this Letter is to illustrate the importance of time-scaling the autocorrelation function to properly compare signals with different spectral properties and jets of different scales. Furthermore, the autocorrelation envelope is implemented as a tool to define a consistent correlation scale in jet noise analysis. These analysis enhancements are first applied to improve understanding of LSS and FSS similarity noise models and then to interpret features of full-scale military jet noise data.

Autocorrelation is a subset of broader correlation analysis techniques, which have long been used to study jet noise fields.^{1,5,6} Several methods have been further developed to better understand sources and mechanisms of laboratory-scale jet noise radiation. Correlation analyses have been used to characterize equivalent sources,^{2,6-8} measure sound speed and associated gradients,⁹ relate flow and acoustic variables,^{3,4,10-12} and establish spatiotemporal relationships in the acoustic field.^{2,5} The results of this study may be further applied to characterize features of cross-correlation for laboratory and full-scale jet data.

Of most relevance to this study is work by Tam *et al.*,¹ who calculated the autocorrelation from far-field pressure measurements of a laboratory-scale jet to develop correlation length scales and draw conclusions about the physical size of the

“energetic acoustic pulses” radiating from the jet. They showed that the autocorrelation function shapes differed and primary-peak widths for sideline measurements were significantly narrower than those farther downstream. They concluded that these different functional shapes supported their two-source model for FSS radiation to the sideline and for LSS radiation downstream.

One potential challenge with the use of the autocorrelation function to classify FSS and LSS radiation is the dependence of its width on spectral peak frequency and hence, acoustic length scales. For noise spectra with high peak frequencies, the autocorrelation is naturally narrower than for a spectrum dominated by low frequencies. Furthermore, high and low peak frequencies do not uniquely define FSS and LSS radiation—either across a measurement aperture for a single jet or across jets of different scales or conditions. Thus, it is difficult to ascribe autocorrelation width to the *nature* of the radiation.

With these challenges in mind, we approach jet noise analysis via autocorrelation differently than in previous work. In this Letter, the influence of the dominant frequency content on autocorrelation width is mitigated by adjusting autocorrelation time scales by the spectral peak frequency. This scaling facilitates comparisons of autocorrelation calculations across a measurement aperture or different jets. In addition, the amplitude envelopes of these scaled autocorrelation functions are calculated via the Hilbert transform. Use of the amplitude envelope has two advantages. First, the smoothly varying envelope can be displayed logarithmically to more clearly observe low-amplitude features of the autocorrelation. Second, it provides a more consistent analysis tool for investigating and quantifying autocorrelation decay rates. The temporal scaling and autocorrelation envelope developments are discussed further in Sec. 2 and implemented on similarity correlation functions obtained from the inverse Fourier transforms of LSS and FSS similarity spectra defined by Tam *et al.*^{13,14} In Sec. 3, time scaling and envelopes are applied to noise radiation from a static F-22A Raptor and the results are compared to the LSS and FSS envelopes.

2. Methodologies for jet noise autocorrelation analysis

The emphasis of this Letter is the interpretation of the autocorrelation function for physical insight of jet noise. Because the FSS and LSS similarity spectra [shown in Fig. 1(a)] are shaped broadband spectra, rectangular bandpass white noise provides an appropriate analytical model. Specifically, the autocorrelation, $R_{xx}(\tau)$, of bandpass white noise for time delay, τ , is related to both bandwidth, B , and center frequency, f_0 , as¹⁵

$$R_{xx}(\tau) \propto \text{sinc}(\pi B\tau)\cos(2\pi f_0\tau). \tag{1}$$

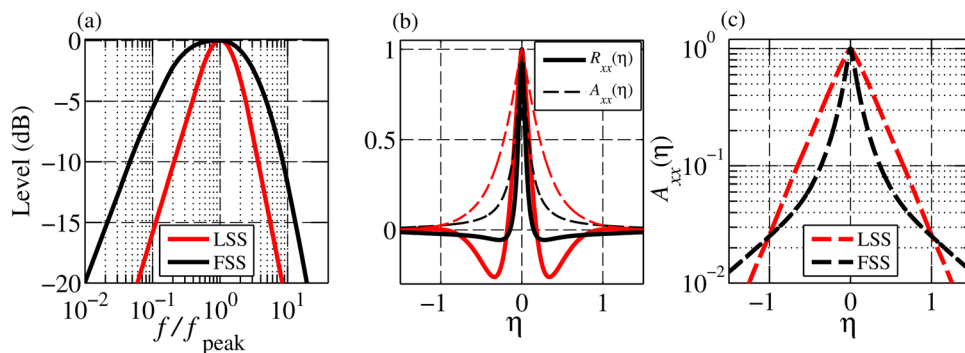


Fig. 1. (Color online) (a) Similarity spectra shapes (Refs. 13 and 14) of the LSS and FSS. (b) Time-scaled autocorrelation coefficient, $R_{xx}(\eta)$, for LSS and FSS radiation, and their envelopes, $A_{xx}(\eta)$. (c) $A_{xx}(\eta)$ for LSS and FSS shown on a logarithmic amplitude scale.

As $B \rightarrow 0$, the sine-wave autocorrelation is recovered: $R_{xx}(\tau) \propto \cos(2\pi f_0 \tau)$. On the other hand, as $B \rightarrow \infty$, $R_{xx}(\tau)$ approaches the delta function expected for white noise. For jet noise, which can be considered a shaped bandpass spectrum, both the spectral width [similar to B in Eq. (1)] and peak frequency (f_{peak} , similar to f_0) directly influence the autocorrelation function. As the spectral width of the jet noise increases, and as peak frequency increases, the autocorrelation function gradually transitions toward a more delta function-like shape.

Time-scaling of the autocorrelation enables greater quantitative physical insight into the nature of the radiated jet sound field. Because f_{peak} and spectral shape vary with location relative to the jet, a time-scaled autocorrelation coefficient, $R_{xx}(\eta)$, where $\eta = \tau f_{\text{peak}}$, is helpful, since it removes the dependence of the autocorrelation width on f_{peak} and leaves the effects of the spectral width. Although a spectrum may not necessarily be centered about f_{peak} , this scaling is usually a good approximation for jet spectra (see, for example, similarity spectra analyses in Ref. 16). Note that Kerhervé *et al.*¹⁷ proposed an inverse Strouhal number time scaling of the autocorrelation to account for differences in jet properties. However, because of the variation in peak frequency with position around the jet, the proposed peak-frequency scaling is more appropriate here to allow for the investigation of FSS and LSS radiation.

Before continuing, it is important to connect the principle of frequency-scaled autocorrelation to the work of Tam *et al.*¹ Although they did not explicitly investigate the effect of f_{peak} on R_{xx} , they recognized the utility of quantifying features of the autocorrelation. They defined a correlation length that is calculated from a time delay corresponding to the maximum anti-correlation multiplied by the speed of sound. However, this was only carried out for LSS signals because it appears that a well-defined anti-correlation does not exist for signals dominated by FSS noise. This difficulty motivates our proposed amplitude envelope function based on the Hilbert transform of the time-scaled autocorrelation coefficient to provide a more consistent analysis technique applicable to both FSS and LSS-dominated signals.

The envelope function of the time-scaled autocorrelation coefficient is defined as¹⁵

$$A_{xx}(\eta) = [R_{xx}^2(\eta) + \tilde{R}_{xx}^2(\eta)]^{1/2}, \quad (2)$$

where $\tilde{R}_{xx}(\eta)$ is the Hilbert transform of the autocorrelation coefficient. Again, this envelope can be used to more consistently quantify differences in the temporal decay rate of $R_{xx}(\eta)$ for various locations around a jet or for jets of different scales and conditions. For example, $A_{xx}(\eta)$ can be used to calculate a characteristic time scale, η_c , from the delays at which $A_{xx}(\eta) = A_{xx}(0)/2$. Additionally, since $A_{xx}(\eta)$ is a positive function, it can be plotted on a logarithmic scale to more clearly observe low-amplitude features not visible in $R_{xx}(\eta)$.

To provide examples of time-scaled autocorrelation functions and corresponding envelopes, we consider the FSS and LSS similarity spectra^{13,14} in Fig. 1(a). The narrower LSS spectrum is more spatially coherent along the jet axis, whereas the broader FSS spectrum is caused by uncorrelated, small-scale turbulent fluctuations throughout the plume.¹ We have calculated inverse Fourier transforms of the analytical FSS and LSS spectra defined by Tam *et al.*^{13,14} for the first time, and the resulting $R_{xx}(\eta)$ are displayed in Fig. 1(b). It is clear that the FSS shape is similar to a white-noise delta-function shape, whereas the LSS $R_{xx}(\eta)$ has larger negative loops, with anti-correlation values less than -0.2 . Note that Tam *et al.*¹ suggested large negative loops in $R_{xx}(\tau)$ were indicative of LSS radiation; Fig. 1(b) shows they were correct. These LSS and FSS-based $R_{xx}(\eta)$ can be used to evaluate autocorrelations in measured jet noise data for properties of FSS and LSS radiation.

The envelopes, $A_{xx}(\eta)$, of the FSS and LSS autocorrelation functions are also displayed in Fig. 1(b), yielding a simpler view of $R_{xx}(\eta)$ features without oscillatory effects. Here it emphasizes the differences in decay of overall correlation between the

LSS and FSS noise, which is not as easily seen with $R_{xx}(\eta)$. The characteristic widths of the FSS and LSS functions are $\eta_c = 0.171$ and $\eta_c = 0.446$, respectively. In Fig. 1(c), the properties of the FSS and LSS envelopes are further examined, with $A_{xx}(\eta)$ plotted on a logarithmic scale. The LSS envelope decays linearly for two orders of magnitude, whereas the FSS envelope has a nonconstant slope with an initially faster decay.

3. Application of autocorrelation analysis to full-scale, high-power jet noise

The methods from Sec. 2 are now applied to measurements¹⁸ of a Pratt and Whitney model F119-PW-100 turbofan engine installed on a static F-22A Raptor [see Fig. 2(a)]. An array of 50 GRAS Type-I 6.35-mm and 3.18-mm microphones [marked by solid dots on Fig. 2(b)] was placed on the ground 11.6 m from the centerline of the jet. Military engine-condition waveforms from microphones located at 90° and 130° (measured relative to the engine inlet and referenced to 5.5 m downstream) are selected for comparison, and their respective one-third octave spectra are given in Fig. 2(c). The spectrum at 130° is of a more peaked nature than the rounded spectrum at 90°. Neilsen *et al.*¹⁶ have shown that the spectrum at 130° is dominated by LSS radiation. At 90°, they show that the overall spectral shape is dictated by FSS radiation, with some influence of LSS radiation in the peak-frequency region.

The autocorrelation coefficients,¹⁵ $R_{xx}(\tau)$, in Fig. 2(d) show that the width of $R_{xx}(\tau)$ at 90° is much narrower than at 130°. Using the length scale developed by Tam *et al.*,¹ the correlation length at 90° is about 0.5 m while at 130° it is about 1.4 m. Although there is significant dissimilarity between these length scales, the difference in peak frequency makes it difficult to draw conclusions relating the length scale and autocorrelation measurements to source characteristics.

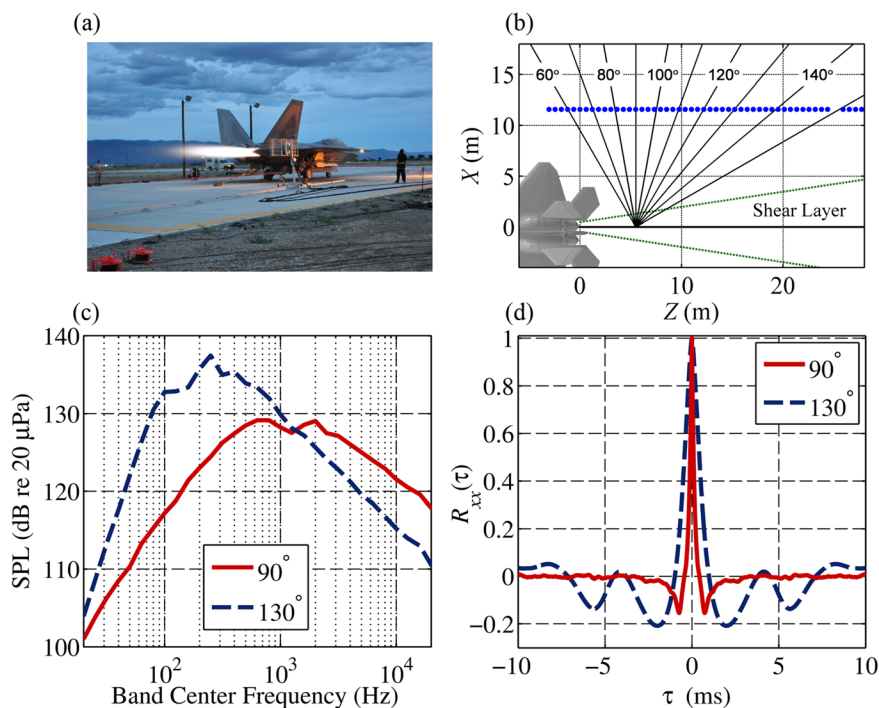


Fig. 2. (Color online) (a) Measurement of an F-22 Raptor at Holloman Air Force base. (b) Measurement schematic of the ground-based array of microphones. Polar angles are measured with respect to the engine inlet and estimated maximum aeroacoustic source region. (c) One-third octave spectra at 90° and 130° positions for a single engine at military power. (d) Autocorrelation coefficient of 90° and 130° waveforms.

The time-scaled $R_{xx}(\eta)$ and $A_{xx}(\eta)$ at 90° and 130° can be used in conjunction with the FSS and LSS functions to interpret the type of acoustic radiation at each measurement angle. Measurements of $R_{xx}(\eta)$ are shown with their respective envelope functions in Figs. 3(a) and 3(b). Once scaled, the time between the negative loops of $R_{xx}(\eta)$ is $\eta \approx 1$ for both measurement angles, providing evidence that the length scale developed by Tam *et al.*¹ is directly related to the spectral peak frequency. At 90° , the shape of $R_{xx}(\eta)$ [in Fig. 3(a)] is similar to $R_{xx}(\eta)$ of FSS from Fig. 1(b); however, the presence of negative loops suggests that the measurement has a small contribution from LSS radiation, as shown by Neilsen *et al.*¹⁶ The corresponding amplitude envelope, $A_{xx}(\eta)$, in Fig. 3(a) has a fairly rapid decay, for which $\eta_c = 0.184$. This matches the FSS η_c to within 8%, suggesting that the LSS radiation does not contribute much to the overall decay in correlation. In Fig. 3(b), $R_{xx}(\eta)$ at 130° contains two pairs of significant negative loops instead of the single set in the LSS function in Fig. 1(b) and seen in the laboratory measurements by Tam *et al.*¹ At this angle, the engine spectrum differs from that of the LSS spectrum in the peak-frequency region due to a significant secondary peak in the spectrum.¹⁹ The double peak spectra may explain the additional pair of loops present here, which cause $A_{xx}(\eta)$ to have a null at $|\eta| \approx 1$ and a subsequent increase in correlation for greater values of η . Even though $A_{xx}(\eta)$ does not decay smoothly at low amplitudes, the measured $\eta_c = 0.514$, which is much larger than η_c of the FSS-dominated 90° measurement and more than 15% greater than the LSS η_c .

To better examine overall features, the $A_{xx}(\eta)$ for the 90° and 130° data are compared against the FSS and LSS envelopes on logarithmic scales in Figs. 3(c) and 3(d). In Fig. 3(c), there is general agreement with the envelope of the 90° measurement and the FSS envelope for nearly two orders of magnitude, which is expected based on agreement in η_c . The negative loops in the autocorrelation coefficient at 90° do not appear to cause significant deviation when the resultant envelope is compared to that of FSS, except for a slightly greater measured correlation than predicted at $|\eta| \approx 0.4$. In Fig. 3(d), the measured $A_{xx}(\eta)$ at 130° has a nearly linear roll-off that agrees fairly

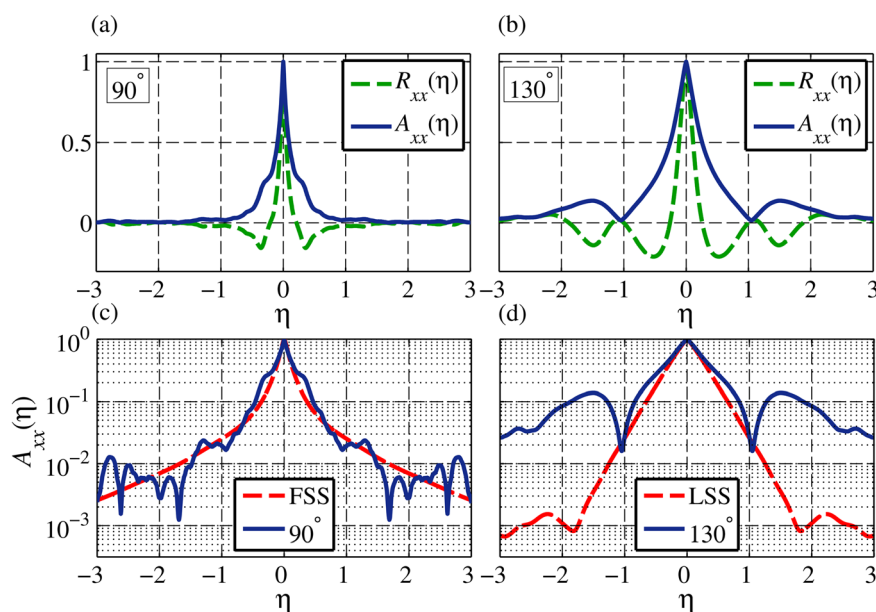


Fig. 3. (Color online) Time-scaled autocorrelation coefficient, $R_{xx}(\eta)$, and their envelopes, $A_{xx}(\eta)$, of the measured waveforms at (a) 90° and (b) 130° . $A_{xx}(\eta)$ is plotted on a logarithmic scale in (c) for 90° along with FSS, and in (d) for 130° along with LSS.

well with the LSS envelope initially, but soon deviates. At $\eta = 2$, there is nearly two orders of magnitude difference between the measured and LSS envelope amplitudes, showing the engine radiation is significantly more correlated over time than for LSS with the same f_{peak} . Therefore, in the maximum radiation region, the characteristics of the jet noise radiation differ appreciably from the LSS model. Note that the change in shape of the LSS envelope at an amplitude of 10^{-3} is consistent with the behavior of $A_{xx}(\eta)$ for rectangular bandpass noise.¹⁵ These comparisons of similarity spectra-based and measured $A_{xx}(\eta)$ have provided additional insight into the nature of the radiated sound field from a full-scale military jet.

4. Conclusion

We have presented methods for applying autocorrelation analysis to jet noise data. A key finding is that the effect of peak frequency on an autocorrelation measurement is removed by appropriate time-scaling, thus allowing for more meaningful comparisons of the autocorrelation across a measurement aperture or different datasets. The Hilbert transform-based envelope function is a useful analysis tool which allows for an explicit, quantitative correlation time scale to be developed irrespective of correlation function shape and low-amplitude features to be more readily visible. As examples of how these analysis techniques are applied, “similarity autocorrelation functions” for large and fine-scale radiation^{13,14} have been presented for the first time. In addition, these techniques have been applied to noise from the F-22A Raptor at sideline and maximum radiation angles at military power. When compared with the similarity functions, the time-scaled autocorrelation coefficient envelope corresponding to the FSS shows good agreement with sideline data. However, in the maximum radiation direction, the envelope for the measured data exhibits regions of higher correlation than the predicted envelope function of the LSS. These methods will be further used to examine radiation properties at other angles and engine conditions and for other jet noise measurements. It is likely similar modifications can be used to extract additional insight from cross-correlation analyses, which is the subject of ongoing work. These analyses may be eventually used to connect the nature of the sound-field radiation and acoustic length scales with the scales of turbulent sources themselves.

Acknowledgments

The authors gratefully acknowledge funding from the Office of Naval Research. The measurements were funded by the Air Force Research Laboratory through the SBIR program and supported through a Cooperative Research and Development Agreement (CRDA) between Blue Ridge Research and Consulting, Brigham Young University, and the Air Force. Distribution A – Approved for Public Release; Distribution is Unlimited 88ABW-2012-6367.

References and links

- ¹C. K. W. Tam, K. Viswanathan, K. K. Ahuja, and J. Panda, “The sources of jet noise: Experimental evidence,” *J. Fluid Mech.* **615**, 253–292 (2008).
- ²K. Viswanathan, J. R. Underbrink, and L. Brusniak, “Space-time correlation measurements in near fields of jets,” *AIAA J.* **49**, 1577–1599 (2011).
- ³P. J. Morris and K. B. M. Q. Zaman, “Velocity measurements in jets with application to noise source modeling,” *J. Sound Vib.* **329**, 394–414 (2010).
- ⁴S. Karabasov, M. Afsar, T. Hynes, A. Dowling, W. McMullan, C. Pokora, G. Page, and J. McGuirk, “Jet noise: Acoustic analogy informed by large eddy simulation,” *AIAA J.* **48**, 1312–1325 (2010).
- ⁵B. L. Clarkson, “Correlation of pressures around a jet engine,” *Proceedings of WADC University of Minnesota Conference on Acoustical Fatigue*, WADC TR 59-676 (March 1961), pp. 85–98.
- ⁶H. V. Fuchs, “Space correlations of the fluctuating pressure in subsonic turbulent jets,” *J. Sound Vib.* **23**, 77–99 (1972).
- ⁷H. V. Fuchs, “Application of acoustic mirror, telescope and polar correlation techniques to jet noise source location,” *J. Sound Vib.* **58**, 117–126 (1978).

- ⁸M. J. Fisher, M. Harper-Bourne, and S. A. L. Glegg, "Jet engine noise source location: The polar correlation technique," *J. Sound Vib.* **51**, 23–54 (1977).
- ⁹W. J. Baars, C. E. Tinney, N. E. Murray, B. J. Jansen, and P. Panickar, "The effect of heat on turbulent mixing noise in supersonic jets," Paper No. 2011-1029, AIAA, 2011.
- ¹⁰J. Panda, R. G. Seasholtz, and K. A. Elam, "Investigation of noise sources in high-speed jets via correlation measurements," *J. Fluid Mech.* **537**, 349–385 (2005).
- ¹¹J. Panda and R. G. Seasholtz, "Experimental investigation of density fluctuations in high-speed jets and correlation with generated noise," *J. Fluid Mech.* **450**, 97–130 (2002).
- ¹²M. J. Doty and D. K. McLaughlin, "Space-time correlation measurements of high-speed axisymmetric jets using optical deflectometry," *Exp. Fluids* **38**, 415–425 (2005).
- ¹³C. K. W. Tam, M. Golebiowski, and J. M. Seiner, "On the two components of turbulent mixing noise from supersonic jets," Paper No. 96-1716, AIAA, 1996.
- ¹⁴C. K. W. Tam and K. B. M. Q. Zaman, "Subsonic jet noise from nonaxisymmetric and tabbed nozzles," *AIAA J.* **38**, 592–599 (2000).
- ¹⁵J. S. Bendat and A. G. Piersol, *Random Data: Analysis and Measurement Procedures*, 4th ed. (Wiley, Hoboken, NJ, 2010), pp. 109–503 (the autocorrelation is calculated using the autospectral density estimate as explained in Sec. 11.4.2).
- ¹⁶T. B. Neilsen, K. L. Gee, A. T. Wall, and M. M. James, "Similarity spectra analysis of high-performance jet aircraft noise," *J. Acoust. Soc. Am.* **133**, 2116–2125 (2013).
- ¹⁷F. Kerhervé, A. Guitton, P. Jordan, J. Delville, V. Fortuné, Y. Gervais, and C. Tinney, "Identifying the dynamics underlying the large-scale and fine-scale jetnoise similarity spectra," Paper No. 2008-3027, AIAA, 2008.
- ¹⁸A. T. Wall, K. L. Gee, M. M. James, K. A. Bradley, S. A. McInerny, and T. B. Neilsen, "Near-field noise measurements of a high-performance military jet aircraft," *Noise Control Eng. J.* **60**, 421–434 (2012).
- ¹⁹A. T. Wall, K. L. Gee, T. B. Neilsen, and M. M. James, "Partial field decomposition of jet noise sources using optimally located virtual reference microphones," *Proc. Meet. Acoust.* **18**, 045001 (2012).